# A first principles based polarizable O(N) interatomic force field for bulk silica

J. R. Kermode,[1,a)] S. Cereda,[1] P. Tangney,[2] and A. De Vita[1]
[1]*Department of Physics, King's College London, Strand, London WC2R 2LS, United Kingdom*
[2]*Department of Physics and Department of Materials, Imperial College London, London SW7 2AZ, United Kingdom*

(Received 30 March 2010; accepted 14 July 2010; published online 2 September 2010)

We present a reformulation of the Tangney–Scandolo interatomic force field for silica [J. Chem. Phys. **117**, 8898 (2002)], which removes the requirement to perform an Ewald summation. We use a Yukawa factor to screen electrostatic interactions and a cutoff distance to limit the interatomic potential range to around 10 Å. A reparametrization of the potential is carried out, fitting to data from density functional theory calculations. These calculations were performed within the local density approximation since we find that this choice of functional leads to a better match to the experimental structural and elastic properties of quartz and amorphous silica than the generalized gradient approximation approach used to parametrize the original Tangney–Scandolo force field. The resulting O($N$) scheme makes it possible to model hundreds of thousands of atoms with modest computational resources, without compromising the force field accuracy. The new potential is validated by calculating structural, elastic, vibrational, and thermodynamic properties of $\alpha$-quartz and amorphous silica. © *2010 American Institute of Physics*. [doi:10.1063/1.3475565]

## I. INTRODUCTION

Silica is a material of vast technological importance which has an extremely rich chemical morphology, and a large research effort has been devoted to its experimental investigation[1–8] and to theoretical work based on both empirical interatomic potentials[9–12] and highly accurate *ab initio* calculations.[13–19] The phase diagram of silica is very complex, with a large number of high pressure crystalline polymorphs.[20] In this work, our motivation is to develop a new potential suitable for simulations of crystalline and amorphous silica at low temperatures and pressures. This new potential could be used, for example, within the "learn on the fly" quantum mechanics/molecular mechanics (QM/MM) scheme in studies of fracture,[21] where a quantum mechanical package would be used to describe the bond-breaking processes taking place near the crack tip, leaving the classical potential to describe the elastic response of the surrounding silica matrix.[22] Although first principles quantum mechanical calculations have provided considerable insight into the properties of silica, limitations in the accessible length-scale and time-scale, particularly considering the huge structural complexity of the higher pressure phases, imply that there will always remain a need for accurate interatomic potentials.

Pair potentials of various complexities, often based on the Born–Mayer functional form,[23] have been used to model silica since the early 1980s. Notably, the potential of van Beest, Kramer, and van Santen[10] (referred to as the BKS potential) is a fixed-charge pair potential which remains widely used. However, *ab initio* simulations have revealed that careful inclusion of many-body electrostatic effects is essential to reproduce experimental observables such as the phonon spectrum.[24] While specialized two-body or three-body functional forms have been proposed to describe specific crystal structures,[9] no such recipe is available to deal with the general case of disordered phases such as amorphous silica.

In 2002, Tangney and Scandolo[25] proposed a potential for silica in which the oxygen atoms are polarizable, with dipole moments determined self-consistently in response to the local electrostatic field. The potential was parametrized from *ab initio* forces, energies, and stresses evaluated for an extended database of configurations to achieve enhanced transferability,[26] and has been shown to provide an accurate description of a wide variety of bulk silica properties.[27]

Fitting the parameters of interatomic potentials *ab initio* allows us to test many of the assumptions on which the potential forms are built in a completely unbiased fashion. For example, a common factor linking many silica interatomic potentials is the assumption that a full Ewald sum[28] must be carried out to include long-range electrostatic effects. This summation is computationally very expensive: for three-dimensional systems with periodic boundary conditions, O($N^{3/2}$) scaling with respect to the number of atoms can be achieved by a careful choice of the separation into real-space and reciprocal-space contributions.[29] However, for the two-dimensional geometries widely used in the fracture simulations which motivate this work, it is not possible to improve on O($N^2$) scaling.[11] The computational cost of long-range electrostatics is particularly important for the Tangney-Scandolo (TS) potential since several electric field evaluations are required to self-consistently determine the dipole moments at each time step. It has long been assumed that the slow $(1/r)$ decay of electrostatic interactions makes them

[a)]Electronic mail: james.kermode@kcl.ac.uk.

 

impossible to truncate. However, real materials are not simply composed of rigid ions: electrons screen interactions between nuclei and, as a result of this screening, it is possible to truncate electrostatic interactions for certain systems and for certain physical properties. While there have been very significant developments in the treatment of long-range forces, for example, the O($N \ln N$) particle mesh and O($N$) fast multipole approaches, such methods typically start to outperform Ewald summation only in systems containing more than 100 000 atoms,[30] so it is appropriate to investigate whether an accurate short-range potential can be developed. Previous short-ranged potentials for silica have been developed by applying both Wolf[31] and Yukawa screenings to the BKS functional form.[11] However, these approaches do not include any explicit representation of electronic screening effects. Thus, a polarizable model such as the TS potential should provide a better starting point for developing a short-range potential. We note that transferability problems may be associated with using a potential in a region of phase space far away from where it has been parametrized. It is possible that the screened potential may be less transferable than the one involving a full Ewald summation. We shall therefore restrict ourselves to modeling the dominant low temperature and low-pressure forms of bulk silica, $\alpha$-quartz and amorphous silica, which are the most relevant to fracture calculations. While various attempts have been made to represent surface chemistry processes,[32,33] this is not our intention in this work. Where bond-breaking processes are important, we propose to use this potential within a QM/MM embedding scheme, relying on *ab initio* techniques to describe a small region with high accuracy, with the force field providing the correct elastic environment. In this paper, we present a short-ranged reformulation of the TS potential, together with a reparametrization based on new *ab initio* calculations, followed by various validations of the resulting screened force field. At the time of writing, we became aware of a very recent work[34] based on similar ideas, which does not yet include a reparametrization.

## II. FORCE FIELD

### A. Overview

The potential consists of two parts: a pair potential and dipole polarization of oxygen ions. The pair potential is of Morse–Stretch form, and is unmodified from that used in the original TS form[25]

$$U_{ij}^{\mathrm{sr}} = D_{ij}\left[e^{\gamma_{ij}\left[1-\left(r_{ij}/r_{ij}^{0}\right)\right]} - 2e^{(\gamma_{ij}/2)\left[1-\left(r_{ij}/r_{ij}^{0}\right)\right]}\right], \tag{1}$$

where $U_{ij}^{\mathrm{sr}}$ is the short-ranged contribution to the interaction energy between ions $i$ and $j$, separated by a distance $r_{ij}$ and $D_{ij}$, and $\gamma_{ij}$ and $r_{ij}^{0}$ are parameters specific to the species pair identified by ions $i$ and $j$. The cutoff for this part of the potential is fixed at 18.0 a.u.

The electrostatic contribution to the potential is made up of a sum over pairs of ions, plus a final term to represent the energy required to polarize the ion's electron density

$$U^{\mathrm{el}}(\{q_i,\mathbf{p}_i,\mathbf{r}_i,\alpha_i\}) = \sum_{i=1}^{N}\sum_{j\neq i} U_{ij}^{\mathrm{el}} + \sum_i \frac{p_i^2}{2\alpha_i}. \tag{2}$$

In the original TS potential, the electrostatic pair term is given by

$$U_{ij}^{\mathrm{el}} = \tfrac{1}{2}(E_{qq} + E_{qd} + E_{dd}) \tag{3}$$

and is made up of charge-charge, charge-dipole, and dipole-dipole interactions, denoted by $E_{qq}$, $E_{qd}$, and $E_{dd}$, respectively, and given by

$$E_{qq} = \frac{q_i q_j}{r_{ij}}, \tag{4}$$

$$E_{qd} = \frac{1}{r_{ij}^3}[q_i(\mathbf{p}_j\cdot\mathbf{r}_{ij}) - q_j(\mathbf{p}_i\cdot\mathbf{r}_{ij})], \tag{5}$$

$$E_{dd} = \frac{1}{r_{ij}^3}\left[\mathbf{p}_i\cdot\mathbf{p}_j - \frac{3}{r_{ij}^2}(\mathbf{p}_i\cdot\mathbf{r}_{ij})(\mathbf{p}_j\cdot\mathbf{r}_{ij})\right]. \tag{6}$$

The species charges $q_i$ and polarizabilities $\alpha_i$ are parameters to be determined in the fitting process. The dipole moments $\mathbf{p}_i$ of each polarizable ion are the sum of an induced dipole moment due to the local electrostatic field and a contribution due to the short-range repulsive forces between ions. Following Madden *et al.*,[24] this short-range correction is given by

$$\mathbf{p}_i^{\mathrm{sr}} = \alpha_i \sum_{j\neq i} \frac{q_j \mathbf{r}_{ij}}{r_{ij}^3} g_{ij}(r_{ij}), \tag{7}$$

where

$$g_{ij}(r_{ij}) = c_{ij}\sum_{k=0}^{4}\frac{b_{ij}r_{ij}^k}{k}e^{-b_{ij}r_{ij}}, \tag{8}$$

and $b_{ij}$ and $c_{ij}$ are additional model parameters. The dipole moments are determined at every time step by iterating

$$\mathbf{p}_i^m = \alpha_i \mathbf{E}(\mathbf{r_i};\{\mathbf{p}_j^{m-1}\}_{j\neq i};\mathbf{r}_{j_{j\neq i}}) + \mathbf{p}_i^{\mathrm{sr}} \tag{9}$$

to self-consistency, where $\mathbf{p}_i^m$ is the dipole moment on ion $i$ at iteration $m$ of the self-consistent cycle and $E(\mathbf{r}_i)$ is the total electric field at position $\mathbf{r}_i$ induced by other charges and dipoles. For more information about the self-consistent solution of this equation, see Ref. 25. We note that the derivative of the potential with respect to the self-consistent dipole moments is zero, so there is no need to evaluate the derivative of the dipole moments with respect to ionic positions.

### B. Screened electrostatic interactions

In order to make the potential short-ranged, we apply a Yukawa screening function to Eq. (3), replacing $U_{ij}^{\mathrm{el}}$ with

$$U_{ij}^{\mathrm{el,s}} = \tfrac{1}{2}(E_{qq} + E_{qd} + E_{dd})e^{-\beta r_{ij}} f_c(r_{ij}), \tag{10}$$

where $f_c(r_{ij})$ is a cutoff function which takes the potential smoothly to zero at some distance $r_{\mathrm{cut}}$. We found that the choice of $f_c(r_{ij})$ is not particularly important; we used a simple switching function

$$f_c(r) = \begin{cases} 1, & r < r_{\text{cut}} - d_{\text{cut}}, \\ 1 - \dfrac{r - r_{\text{cut}} + d_{\text{cut}}}{2d_{\text{cut}}} + \dfrac{1}{2\pi}\sin\dfrac{\pi}{d_{\text{cut}}}(r - r_{\text{cut}} + d_{\text{cut}}), & r_{\text{cut}} - d_{\text{cut}} \le r \le r_{\text{cut}} + d_{\text{cut}}, \\ 0, & r > r_{\text{cut}} + d_{\text{cut}}. \end{cases} \tag{11}$$

where $d_{\text{cut}}$ is a smoothing length.

This definition of the screened electrostatic pair interaction energy $U_{ij}^{\text{el,s}}$ is equivalent to transforming the electrostatic Coulomb potential, dipole potential, and dipole field originating from the charge and dipole on each atom $i$. For instance, the transformed short-range potentials are obtained as

$$\Phi_s(\mathbf{r}_i) = \Phi(\mathbf{r}_i)e^{-\beta r_i} f_c(r_i). \tag{12}$$

The appropriate forces corresponding to the transformation are then coded to ensure we have a conservative force field. In particular, the charge-charge, charge-dipole, and dipole-dipole forces have additional contributions which arise from the derivative of the screening functions

$$\mathbf{F}_s^{(ij)} = -\nabla E^{(ij)} e^{-\beta r_{ij}} f_c(r_{ij}), + E^{(ij)}\left(\beta f_c(r_{ij}) - \left.\frac{\mathrm{d}f_c}{\mathrm{d}r}\right|_{r_{ij}}\right)\frac{e^{-\beta r_{ij}}}{r_{ij}}\mathbf{r}_{ij}, \tag{13}$$

where $E^{(ij)}$ is the corresponding, unscreened, energy term from Eqs. (4)–(6). The Yukawa factor $e^{-\beta r_{ij}}$ implies a screening length inversely proportional to $\beta$. Together with the cutoff distance $r_{\text{cut}}$, this parameter will be ultimately determined by the length-scale of physical screening processes which take place in the material.

## III. PARAMETRIZATION

The modified, short-range potential requires a full reparametrization. We have used density functional theory (DFT) to evaluate quantum mechanical forces, energies and stresses on a representative database of atomic configurations. All DFT calculations reported in this work were carried out with the CASTEP planewave code,[35] using ultrasoft pseudopotentials. The TS potential was parametrized using a database generated using a generalized gradient approximation (PBE-GGA) to the exchange-correlation functional.[36,37] Gradient corrections are known to be important for correctly resolving the energy ordering of higher pressure crystalline silica phases.[13,38] However, for modeling fracture processes which take place at relatively low pressures and temperatures, an accurate description of the elastic properties of quartz and low-pressure amorphous silica is our primary motivation. As will be demonstrated below, the local density approximation (LDA) provides a better description of the elastic properties of silica. We therefore decided to carry out the potential reparametrization using the LDA, as discussed in more detail in Sec. IV.

To generate the database, we took a series of around a hundred snapshots from microcanonical molecular dynamics simulations conducted with the original TS potential on a 72-atom quartz unit cell at a temperature of 500 K. To ensure statistical independence, the configurations selected for fitting were separated by several picoseconds. Accurate DFT LDA single-point calculations of forces, energy, and stress were then carried out on each of these snapshots. A relatively high plane-wave cutoff energy of 800 eV was required to fully converge the stress components. Γ-point sampling of the Brillouin zone was found to be sufficient. The potential parameters were then obtained by minimizing the cost function

$$\Gamma[\{\eta_i\}] = w_f \Delta F + w_s \Delta S + w_e \Delta E \tag{14}$$

with respect to the parameters $\{\eta_i\}$, where

$$\Delta F = \frac{\sqrt{\Sigma_{k=1}^{n_c}\Sigma_{i=1}^{N}\Sigma_{\alpha}(F_{cl,i}^{\alpha}(\{\eta_i\}) - F_{ai,i}^{\alpha})^2}}{\sqrt{\Sigma_{k=1}^{n_c}\Sigma_{i=1}^{N}\Sigma_{\alpha}(F_{ai,i}^{\alpha})^2}}, \tag{15}$$

$$\Delta S = \frac{\sqrt{\Sigma_{k=1}^{n_c}\Sigma_{\alpha,\beta}(\sigma_{cl}^{\alpha,\beta}(\{\eta_i\}) - \sigma_{ai}^{\alpha,\beta})^2}}{3B\sqrt{n_c}}, \tag{16}$$

$$\Delta E = \frac{\sqrt{\Sigma_{k,l}^{n_c}((U_k^{cl} - U_l^{cl}) - (U_k^{ai} - U_l^{ai}))^2}}{\sqrt{\Sigma_{k,l}^{n_c}(U_k^{ai} - U_l^{ai})^2}}. \tag{17}$$

The outermost sum is over the $n_c$ distinct configurations, labeled by $k$. $F_{cl,i}^{\alpha}$ is the $\alpha$-component of the force on ion $i$ calculated with the classical potential using parameters $\{\eta_i\}$; $F_{ai,i}^{\alpha}$ is the $\alpha$-component of the force on ion $i$ calculated *ab initio*; $\sigma_{cl}^{\alpha,\beta}$ are the components of the stress tensor calculated with the classical potential; $B$ is the bulk modulus; $\sigma_{ai}^{\alpha,\beta}$ are the components of the *ab initio* stress tensor; $U_k^{cl}$ is the en-

TABLE I. Potential parameters (atomic units).

| Parameter | O–O | Si–O | Si–Si |
|---|---|---|---|
| $D_{ij}$ | 0.000 307 | 0.002 012 | 0.339 67 |
| $\gamma_{ij}$ | 12.16 | 11.35 | −0.17 |
| $r_{ij}^0$ | 7.02 | 4.57 | −0.08 |
| $b_{ij}$ | 1.12 | 1.97 | 0.0 |
| $c_{ij}$ | 0.44 | −1.50 | 0.0 |

| Parameter | O | Si |
|---|---|---|
| $\alpha_i$ | 14.13 | 0.0 |
| $q_i$ | −1.43 | 2.86 |

| Parameter | Value |
|---|---|
| $\beta$ | 0.1 |
| $r_{\text{cut}}$ | 20.0 |
| $d_{\text{cut}}$ | 10.0 |

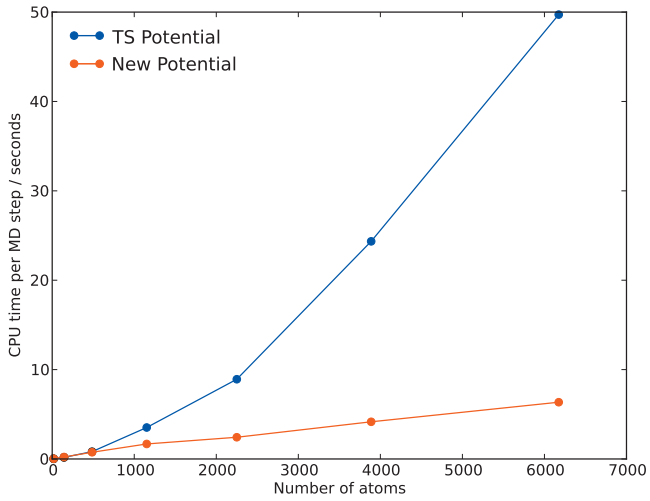


FIG. 1. Time taken for a single MD step as a function of number of atoms, with the original TS potential (blue) and with the new Yukawa-screened implementation (red).

ergy of configuration $k$ computed with the classical potential; and $U_k^{ai}$ is its *ab initio* energy. The weights $w_f$, $w_s$, and $w_e$ are chosen to reflect the amount of information available, e.g., always implying that $w_f > w_s > w_e$ (a typical choice is $w_f = 1.0$, $w_s = 0.5$, and $w_e = 0.1$). The minimization process is described in more detail in Ref. 39.

After identifying the set of parameters that minimizes $\Gamma[\{\eta_i\}]$, we used it to carry out a molecular dynamics simulation to generate a new set of reference configurations. The fitting process is then iterated until no systematic parameter change is detectable. This procedure is designed to ensure that the configurations used are representative samples without incurring the computational expense of carrying out long *ab initio* molecular dynamics simulations.[26] For this potential, the fitting process was expedited by the existence of a good set of starting configurations generated with the original TS potential.

The Yukawa screening parameters $\beta$ and $r_{\text{cut}}$ were not directly included in the fitting process. Instead, a range of values were tried, from which the inverse length $\beta = 0.1$ a.u.$^{-1}$ and the cutoff radius $r_{\text{cut}} = 20$ a.u. were selected as the best compromise between computational efficiency and fit accuracy. In a similar manner, the distance over which the smoothing function $f_c(r)$ goes to zero was chosen to be $d_{\text{cut}} = 10$ a.u. The final set of parameters (Table I) selected yields the values $\Delta F = 0.10$, $\Delta S = 0.001$, and $\Delta E = 0.25$ for the three positive definite error components of our cost function. This compares well with the original TS potential which has $\Delta F = 0.16$, $\Delta S = 0.014$, and $\Delta E = 0.18$, albeit for a QM database sampled from higher temperature dynamical simulations of the liquid, where forces tend to be larger. To summarize, by introducing the screening and specializing the fit for lower temperature configurations, we have obtained a low force and stress error and a slightly increased error in the energies. This is suitable for use within a force-mixing based QM/MM framework[40] such as the learn on the fly method[21] where force accuracy is paramount.

## IV. RESULTS

### A. Implementation

The screened version of the TS potential is significantly faster than the original and, crucially, the finite range leads to linear scaling with respect to the number of atoms. As shown in Fig. 1, a speed up of more than one order of magnitude is achieved for a 6000 atom system. For systems containing fewer than ~500 atoms, the early TS potential, which does not involve additional screening terms and their derivatives, is actually faster than our novel formulation. The new potential has been implemented within the QUIP (Ref. 41) molecular dynamics framework and has been parallelized, resulting in a code which exhibits linear scaling with respect to both number of atoms and number of CPUs. The implementation has been verified by tightening the convergence tolerance of the self-consistent determination of the dipole moments and checking that the drift in total energy can be made arbitrarily small. Force evaluation carried out with new potential has a computational cost of the order of $10^{-4}$ s/atom on four cores of a 3 GHz Intel "Woodcrest" machine, making simulations with hundreds of thousands of atoms easily affordable.

### B. Structural and elastic properties of quartz

The structural and elastic properties of $\alpha$-quartz have been calculated using our new potential and are reported in Tables II and III, together with the DFT LDA and PBE-GGA values. A $5\times5\times4$ Monkhorst–Pack **k**-point mesh was used for the DFT structural optimizations. Quartz has trigonal symmetry; the most stable form at temperatures below around 500 °C is $\alpha$-quartz which is a member of the $P3_221$ space group. Its primitive cell is illustrated in Fig. 2. The quartz lattice parameters $a$ and $c$ and the internal parameters $u$, $x$, $y$, and $z$ were determined by geometry optimization, where $(u,0,2/3)$ and $(x,y,2/3+z)$ are the fractional coordi-

TABLE II. Structural properties of $\alpha$-quartz.

| | Experiment[a] | DFT (LDA) | DFT (PBE-GGA) | TS potential | New potential |
|---|---|---|---|---|---|
| $a$/Å | 4.9160 | 4.8701 | 5.0284 | 4.9034 | 4.8409 |
| $c$/Å | 5.4054 | 5.3626 | 5.5120 | 5.3810 | 5.3285 |
| V/$SiO_2$/Å$^3$ | 37.71 | 36.71 | 40.23 | 37.35 | 36.05 |
| Si $u$ | 0.4697 | 0.4667 | 0.4813 | 0.4706 | 0.4641 |
| O $x$ | 0.4135 | 0.4129 | 0.4165 | 0.4140 | 0.4118 |
| O $y$ | 0.2669 | 0.2720 | 0.2466 | 0.2681 | 0.2788 |
| O $z$ | 0.1191 | 0.1159 | 0.1360 | 0.1182 | 0.1097 |

[a]Reference 7.

TABLE III. Elastic constants of $\alpha$-quartz in GPa.

| | Experiment[a] | Experiment[b] | DFT (LDA) | DFT (PBE-GGA) | TS potential | New potential |
|---|---|---|---|---|---|---|
| $C_{11}$ | 85.9 | 86.8 | 76.6 | 87.1 | 98.5 | 83.5 |
| $C_{12}$ | 7.16 | 7.04 | 5.88 | −7.82 | 15.2 | 12.7 |
| $C_{13}$ | 10.94 | 11.91 | 6.58 | 6.30 | 26.1 | 14.6 |
| $C_{14}$ | −17.66 | −18.04 | −17.8 | −17.0 | −10.5 | −16.9 |
| $C_{33}$ | 89.59 | 105.75 | 95.9 | 87.1 | 111.1 | 118.1 |
| $C_{44}$ | 57.77 | 58.2 | 54.1 | 49.1 | 59.8 | 59.06 |
| $C_{66}$ | 39.4 | 39.9 | 35.3 | 47.5 | 41.6 | 35.41 |

[a]Reference 4.
[b]Reference 5.

nates of the first silicon and oxygen atoms, respectively, and the other positions are constrained by symmetry requirements. The minimum in the potential energy surface of our new potential obeys the required symmetry operations for the $P3_221$ space group to a precision of better than $10^{-5}$ Å. The crystallographic symmetry group to which quartz belongs has five independent elastic constants: $C_{11}$, $C_{12}$, $C_{14}$, $C_{33}$, and $C_{44}$ [$C_{66}$ is then given by $(C_{11}-C_{12})/2$]. The $C_{ij}$ were computed using a series of finite strains and the virial stress. The internal coordinates of each strained configuration were each time fully relaxed.

The DFT values reported in Tables II and III agree well with experiment and with previously published *ab initio* results.[13–18] The LDA consistently underestimates the equilibrium volume of quartz compared with experiment, whereas the PBE-GGA overestimates by a slightly larger factor, leading to increased errors in the elastic properties with respect to experiment.[13] This point is further illustrated by considering a third-order fit to the Murnaghan equation of state. We found that both approximations to the exchange-correlation energy lead to accurate predictions of the bulk modulus: 31.7 GPa with the LDA and 29.3 GPa with the PBE-GGA, compared to an experimental range of 34–37 GPa.[13] However, the variation in the derivative of the bulk modulus with respect to pressure between LDA and PBE-GGA is more significant. Our results are 5.56 within the LDA and 4.43 with the PBE-GGA, to be compared with the experimental value of $B'=5.99$.[13] In general, the PBE-GGA functional is less accurate at predicting quartz elastic properties,[13,15] which supports our decision to use the LDA to reparametrize our potential. The elastic constants predicted by the new potential are in excellent agreement with both DFT LDA and experiment. It is worth noting that the accuracy of the force fit ($\Delta F=0.10$) in the parametrization of our potential is comparable to or larger than the likely differences between the forces predicted by different approximations to the exchange-correlation energy, whereas the relative error in the stress ($\Delta S=0.001$) is much lower and is likely to be smaller than the differences between different functionals. Since the elastic constants predicted by the LDA are in good agreement with experiment, we chose to parametrize our potential using this functional. To summarize our results so far, improvement over the TS potential with respect to experiment can be attributed to the use of LDA for the fit and to the choice of a more specialized fit database: the new potential has been fit to crystal configurations at 500 K, whereas the original TS was fit to liquid silica at 3000 K. We have checked this by refitting the original TS functional form, including long-range electrostatics, to the same LDA database. This leads to a potential which provides an almost identical description of quartz to our screened potential, indicating that the variations between the TS and Yukawa-screened potentials are primarily due to the choice of QM database and that truncation of the long-range electrostatic interactions does not significantly affect the accuracy of the potential, in agreement with a very recent similar work.[34]

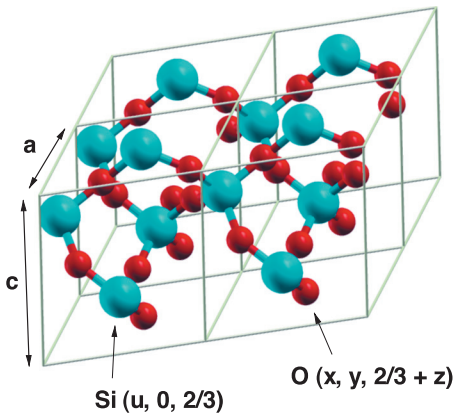


FIG. 2. $2\times2\times1$ supercell of the $\alpha$-quartz primitive cell, showing the lattice parameters $a$ and $c$ and the internal coordinates $u$, $x$, $y$, and $z$. Silicon atoms are blue and oxygen atoms red.

### C. Vibrational properties

We calculated the phonon dispersion spectrum of $\alpha$-quartz predicted by the new potential using PHONOPY,[42] which uses the supercell method with finite atomic displacements,[43] and the Parlinski–Li–Kawasoe interpolation scheme.[44] The results shown in Fig. 3 were obtained with a $4\times4\times4$ supercell of the nine-atom primitive unit cell. This is sufficient to converge the components of the force constant matrix, confirming that the screened potential's cutoff distance of $r_{cut}=20$ a.u. is reasonable.

Overall, the agreement with experiment and with density functional perturbation theory (DFPT) is good, particularly for the low-frequency transverse modes. Even for the longitudinal optical modes where long-range electrostatic effects are more important, the screened potential does not perform significantly worse than the TS potential. In fact, the optical

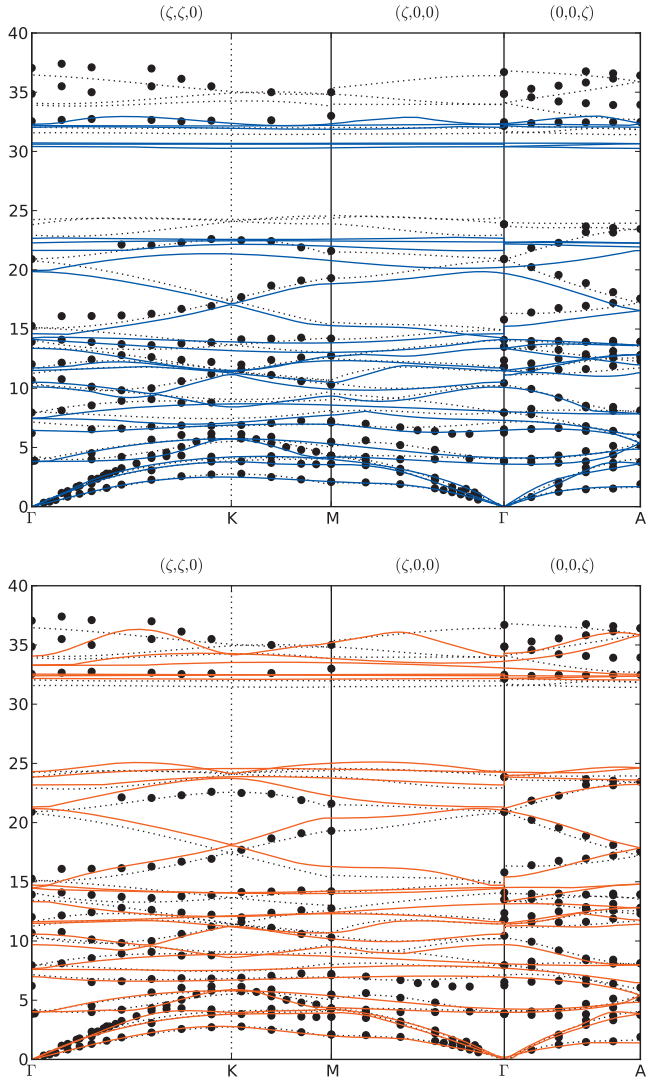


FIG. 3. Phonon dispersion curves for $\alpha$-quartz predicted by the TS potential and the new parametrization (solid blue and red lines, respectively) compared to experiment (Refs. 1 and 2) (black circles) and DFPT LDA (black dashed lines) data reproduced from Ref. 15. $\Gamma$, $K$, $M$, and $A$ are special points in the Brillouin zone with coordinates (0,0,0), (2/3,0,0), (1/2,0,0), and (0,0,1/2), respectively.

modes are described slightly better with the new potential than with the original. This is not unexpected: the original potential was fitted to PBE-GGA data, and a recent study computed the GGA phonon spectrum of $\alpha$-quartz and found the agreement with the same experimental data to be slightly worse than that of LDA calculations.[45] We note that phonon modes with wavelengths longer than the range of the potential cannot be correctly described by a screened model, but we do not expect long wavelength optical modes to play an important role in typical molecular dynamics simulations using this potential. The longitudinal frequencies near the $\Gamma$-point have been corrected by adding the nonanalytic contribution due to long-range electric fields to the dynamical matrix.[46] This requires calculating the high-frequency dielectric tensor $\epsilon_\infty$ and the Born effective charge tensor $\mathbf{Z}^*$. Following the approach taken by Han *et al.*,[47] this has been done by direct evaluation of the polarization response to small external electric fields (for $\epsilon_\infty$) and to small atomic displacements (for $\mathbf{Z}^*$); the results are presented in Tables IV and V. The DFT values were computed with the CASTEP code using DFPT.[45]

The agreement between the dielectric relative permittivities calculated with the new potential and DFT LDA is good. Note that once more the TS potential agrees better with the PBE-GGA results. However, for both potentials, the Born effective charge tensors do not agree particularly well with the *ab initio* values. This suggests that the functional form of our potential does not describe the full range of possible electron response phenomena. Since the Born effective charges predicted by the model are too small, the longitudinal optical/transverse optical (LO/TO) splittings at the $\Gamma$-point are also significantly lower than those calculated *ab initio* or experimentally measured. This reflects the fact that long-range forces between ions are determined by the screened effective charge tensor $Z^*_{\alpha\beta}/\sqrt{\epsilon_{\gamma\delta}}$.[47] For $\alpha$-quartz,

TABLE V. High-frequency dielectric permittivities of $\alpha$-quartz.

| | $\epsilon^\infty_\parallel$ | $\epsilon^\infty_\perp$ |
|---|---|---|
| Experiment[a] | 2.383 | 2.356 |
| DFT LDA (this work) | 2.63 | 2.59 |
| DFT PBE-GGA[b] | 2.404 | 2.381 |
| TS potential | 2.31 | 2.31 |
| New potential | 2.50 | 2.49 |

[a]Reference 3.
[b]Reference 45.

TABLE IV. Born effective charge tensors for the silicon atom with fractional coordinates $(u,0,2/3)$ and the oxygen atom at $(x,y,2/3+z)$ in the $\alpha$-quartz primitive cell (atomic units).

| | Silicon | | | Oxygen | | |
|---|---|---|---|---|---|---|
| | 3.50 | 0.31 | 0.26 | −1.41 | −0.60 | −0.55 |
| DFT (LDA) | 0.31 | 3.14 | 0.15 | −0.54 | −1.91 | −0.64 |
| | −0.31 | −0.18 | 3.45 | −0.48 | −0.68 | −1.73 |
| | 2.13 | 0.07 | 0.05 | −0.93 | −0.22 | −0.25 |
| TS potential | 0.07 | 2.05 | 0.03 | −0.23 | −1.16 | −0.24 |
| | −0.12 | −0.07 | 2.13 | −0.21 | −0.25 | −1.06 |
| | 2.36 | 0.06 | 0.04 | −1.06 | −0.21 | −0.25 |
| New potential | 0.06 | 2.29 | 0.03 | −0.22 | −1.27 | −0.20 |
| | −0.12 | −0.07 | 2.36 | −0.21 | −0.22 | −1.18 |

TABLE VI. Nonzero components of the screened effective charge tensor $Z^*_{\alpha\beta}/\sqrt{\epsilon_{\gamma\delta}}$ for $\alpha$-quartz for the silicon atom with fractional coordinates $(u,0,2/3)$ and the oxygen atom at $(x,y,2/3+z)$, in atomic units.

| | DFT (LDA) | | TS potential | | New potential | |
|---|---|---|---|---|---|---|
| $\alpha\beta\gamma\delta$ | Si | O | Si | O | Si | O |
| 1111 | 2.175 | −0.875 | 1.402 | −0.611 | 1.495 | −0.670 |
| 1133 | 2.161 | −0.869 | 1.400 | −0.610 | 1.493 | −0.669 |
| 1211 | 0.193 | −0.375 | 0.044 | −0.146 | 0.038 | −0.131 |
| 1233 | 0.192 | −0.373 | 0.044 | −0.146 | 0.038 | −0.131 |
| 1311 | 0.164 | −0.339 | 0.033 | −0.166 | 0.028 | −0.158 |
| 1333 | 0.163 | −0.337 | 0.033 | −0.166 | 0.028 | −0.157 |
| 2111 | 0.193 | −0.338 | 0.044 | −0.152 | 0.038 | −0.140 |
| 2133 | 0.192 | −0.336 | 0.044 | −0.152 | 0.038 | −0.140 |
| 2211 | 1.952 | −1.189 | 1.351 | −0.766 | 1.451 | −0.803 |
| 2233 | 1.939 | −1.181 | 1.349 | −0.765 | 1.449 | −0.801 |
| 2311 | 0.095 | −0.398 | 0.019 | −0.156 | 0.016 | −0.129 |
| 2333 | 0.094 | −0.395 | 0.019 | −0.156 | 0.016 | −0.129 |
| 3111 | −0.191 | −0.295 | −0.081 | −0.139 | −0.076 | −0.131 |
| 3133 | −0.190 | −0.293 | −0.081 | −0.138 | −0.076 | −0.131 |
| 3211 | −0.111 | −0.419 | −0.047 | −0.170 | −0.044 | −0.142 |
| 3233 | −0.110 | −0.417 | −0.046 | −0.170 | −0.044 | −0.142 |
| 3311 | 2.143 | −1.071 | 1.399 | −0.700 | 1.497 | −0.748 |
| 3333 | 2.128 | −1.064 | 1.398 | −0.699 | 1.495 | −0.747 |

symmetry dictates that this tensor has 18 independent components, the values of which are given in Table VI for DFT, the TS potential, and our new screened potential. While the agreement between DFT and either potential is not very good, the two potentials are quite consistent with one another. This suggests that it is the still somewhat limited functional form, rather than the inclusion or exclusion of long-range electrostatic interactions, which is preventing a greater accuracy.

### D. Amorphous silica

The new potential has also been tested for amorphous silica. We obtained amorphous structures following the approach of Ref. 48. In particular, we slightly distorted a 576 atom $\alpha$-quartz cell to make it cubic, setting the density to the experimental value of 2.2 $g/cm^3$. The system was initially thermalized at 5000 K for 50 ps and then cooled down to room temperature at an annealing rate of 0.01 K/fs. The 0.1 fs time step used for the high temperatures regime was sufficiently small to guarantee energy conservation within $10^{-6}$ $k_BT/ps$. The final 300 K configuration was then structurally optimized, relaxing both the lattice vectors and the atomic positions. The elastic properties of the optimized configuration, as obtained with the new potential and the original TS potential, are shown in Table VII. As was the case for $\alpha$-quartz, the agreement with experiment improves slightly using the new LDA-fitted potential. The system was, at this point, annealed back to room temperature and, successively, at $T=3000$ K to evaluate its dynamical structural properties. In Fig. 4 we compare the radial distribution functions predicted by the two potentials computed at $T=300$ K and $T=3000$ K for the Si–Si and O–O coordinations. While very good agreement is obtained throughout, the two potentials compare better at room temperature than at 3000 K. We also thermalized the amorphous system at significantly higher temperatures, up to 5000 K, and found a slightly worsened agreement with the TS potential. This is not unexpected, since the new potential was parametrized including fewer distorted configurations in the fit database, making it slightly less suitable for describing the high temperature liquid phase.

Si–O–Si bond angle distributions obtained at 300 K using the two potentials are shown in Fig. 5. These distributions were obtained from 100 ps long *NVT* molecular dynamics simulations carried out after independent structural and cell optimizations starting from the same 72-atom amorphous configuration. Since the volume and shape of the simulation cell play a role in determining the shape of the bond angle distribution, this procedure is expected to reveal possible discrepancies between the original TS and our new potential. Moreover, the small cell size used in this test allows direct comparison with the distribution produced by a reference 14 ps long first principles simulation. This is also shown in Fig. 5, revealing that while the two classical potentials are reasonably consistent with one another, their difference is of roughly the same magnitude as their discrepancy from the LDA results and the discrepancy between LDA and GGA presented in Ref. 49. This suggests that the new linear

TABLE VII. Equilibrium density and elastic properties of amorphous silica.

| | Experiment | TS potential | New potential |
|---|---|---|---|
| Density $(g/cm^3)$ | 2.20[a] | 2.26 | 2.26 |
| Bulk modulus $B$ (GPa) | 38.0[b] | 43.3 | 36.9 |
| Young's modulus $E$ (GPa) | 69.1[b] | 74.3 | 69.1 |
| Poisson ratio $\nu$ | 0.197[b] | 0.166 | 0.174 |
| $C_{11}$ (GPa) | 76.5[b] | 81.6 | 73.7 |
| $C_{12}$ (GPa) | 18.8[b] | 25.6 | 21.7 |
| $C_{44}$ (GPa) | 28.9[b] | 32.1 | 30.1 |

[a]Experimental data from Ref. 8
[b]Experimental data from Ref. 6 at temperature of 77 K.

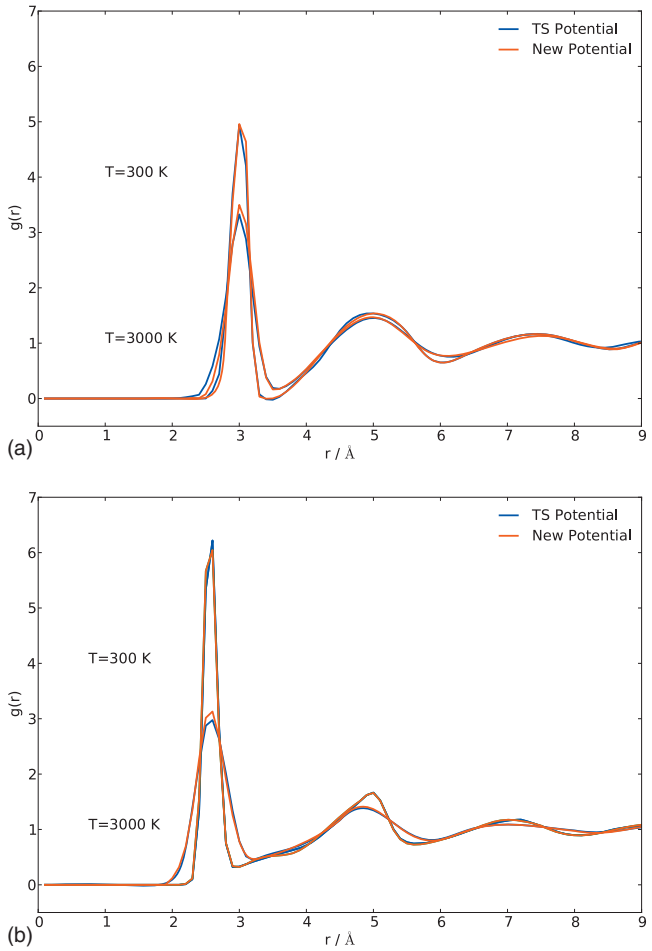


FIG. 4. Radial distribution function for (a) Si–Si and (b) O–O as computed at two different temperatures $T=300$ K and $T=3000$ K.

scaling potential describes amorphous silica at low temperatures no less accurately than the original one. We note that fixing the cell as we do in our *NVT* simulations may slightly bias the Si–O–Si distribution toward larger angles,[49] so that the distributions obtained cannot be expected to fully match that of real silica.

At room temperature and below, almost all silicon atoms within the amorphous structure are fourfold coordinated. We occasionally observe defects, principally threefold and fivefold coordinated atoms, and even less frequently we detect two-membered silicon rings with the structure previously reported in *ab initio* surface calculations.[19] While two-membered rings are almost never encountered in the bulk, they are known to play an important role in chemical processes on amorphous silica surfaces, for which they are thought to provide the main reaction sites.[50] We have tested our potential on the dehydrogenated amorphous surface and we observe the systematic formation of two-membered rings which remain stable at room temperature.

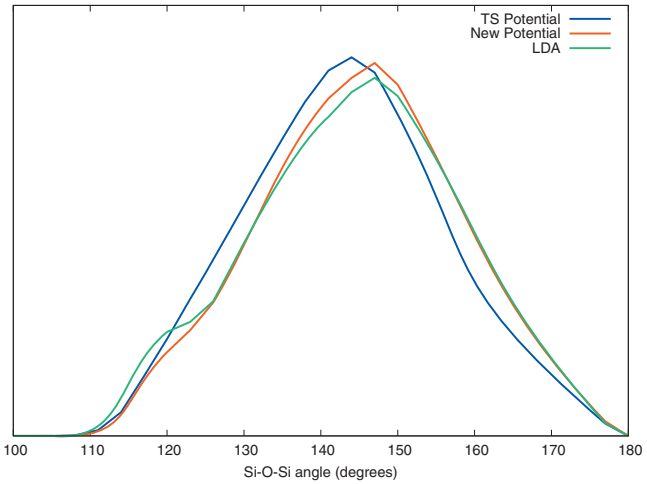


FIG. 5. Si–O–Si bond angle distributions for the two potentials and DFT LDA, computed at a temperature of $T=300$ K.

## V. CONCLUSIONS

We have developed a short-ranged version of the Tangney and Scandolo polarizable potential for silica, reparametrized from first principles calculations without any reliance on experimental data. Despite an effective cutoff distance of ~10 Å, our potential reproduces *ab initio* and experimental structural, elastic, and vibrational properties of both $\alpha$-quartz and amorphous silica to a high degree of accuracy. Due to its short range, our potential is linear scaling with respect to the number of atoms in the simulation and is thus suitable for modeling extended systems.

## ACKNOWLEDGMENTS

J.R.K. and A.D.V. acknowledge funding from the Rio Tinto Centre for Advanced Mineral Recovery, based at Imperial College, London. P.T. acknowledges support from the European Commission within the Marie Curie Support for Training and Development of Researchers Programme under Contract No. MIRG-CT-2007-208858. S.C. and A.D.V. acknowledge funding from the EU-FP7-NMP Grant "ADGLASS."

[1] B. Dorner, H. Grimmt, and H. Rzanyg, J. Phys. C **13**, 6607 (1980).
[2] B. Dorner and D. Strauch, J. Phys.: Condens. Matter **5**, 6149 (1993).
[3] F. Gervais and B. Piriou, Phys. Rev. B **11**, 3944 (1975).
[4] E. Gregoryanz, R. Hemley, H.-K. Mao, and P. Gillet, Phys. Rev. Lett. **84**, 3117 (2000).
[5] H. J. McSkimin, P. Andreatch, and R. N. Thurston, J. Appl. Phys. **36**, 1624 (1965).
[6] Q. Wang, G. Saunders, H. Senin, and E. Lambson, J. Non-Cryst. Solids **143**, 65 (1992).
[7] L. Levien, C. T. Prewitt, and D. J. Weidner, Am. Mineral. **65**, 920 (1980).
[8] R. Brückner, J. Non-Cryst. Solids **5**, 123 (1970).
[9] P. Vashishta, R. Kalia, J. Rino, and I. Ebbsjö, Phys. Rev. B **41**, 12197 (1990).
[10] B. van Beest, G. Kramer, and R. van Santen, Phys. Rev. Lett. **64**, 1955 (1990).
[11] A. Carré, L. Berthier, J. Horbach, S. Ispas, and W. Kob, J. Chem. Phys. **127**, 114512 (2007).
[12] J. Horbach and W. Kob, Phys. Rev. B **60**, 3169 (1999).
[13] T. Demuth, Y. Jeanvoine, J. Hafner, and J. Angyan, J. Phys.: Condens. Matter **11**, 3833 (1999).
[14] M. Catti, B. Civalleri, and P. Ugliengo, J. Phys. Chem. B **104**, 7259 (2000).
[15] N. Choudhury and S. Chaplot, Phys. Rev. B **73**, 094304 (2006).
[16] B. Holm and R. Ahuja, J. Chem. Phys. **111**, 2071 (1999).
[17] N. Flocke, W. Zhu, and S. B. Trickey, J. Phys. Chem. B **109**, 4168 (2005).
[18] H. Kimizuka, S. Ogata, J. Li, and Y. Shibutani, Phys. Rev. B **75**, 054109 (2007).

[19] D. Ceresoli, M. Bernasconi, S. Iarlori, M. Parrinello, and E. Tosatti, Phys. Rev. Lett. **84**, 3887 (2000).
[20] R. Hemley, J. Badrom, and D. Teter, in *Physics Meets Mineralogy: Condensed-Matter Physics in Geosciences*, edited by H. Aoki and Y. Syono (Cambridge University Press, New York, 2000), pp. 173–204.
[21] G. Csányi, T. Albaret, M. Payne, and A. De Vita, Phys. Rev. Lett. **93**, 175503 (2004).
[22] J. R. Kermode, T. Albaret, D. Sherman, N. Bernstein, P. Gumbsch, M. C. Payne, G. Csányi, and A. De Vita, Nature (London) **455**, 1224 (2008).
[23] N. March and M. Tosi, *Coulomb Liquids* (Academic, London, 1984).
[24] A. Rowley, P. Jemmer, M. Wilson, and P. Madden, J. Chem. Phys. **108**, 10209 (1998).
[25] P. Tangney and S. Scandolo, J. Chem. Phys. **117**, 8898 (2002).
[26] A. Laio, S. Bernard, G. Chiarotti, S. Scandolo, and E. Tosatti, Science **287**, 1027 (2000).
[27] D. Herzbach, K. Binder, and M. H. Muser, J. Chem. Phys. **123**, 124711 (2005).
[28] P. Ewald, Ann. Phys. **64**, 253 (1921).
[29] J. Perram, H. Petersen, and S. De Leeuw, Mol. Phys. **65**, 875 (1988).
[30] K. Esselink, Comput. Phys. Commun. **87**, 375 (1995).
[31] D. Wolf, P. Keblinski, S. R. Phillpot, and J. Eggebrecht, J. Chem. Phys. **110**, 8254 (1999).
[32] A. Pedone, G. Malavasi, M. C. Menziani, U. Segre, F. Musso, M. Corno, B. Civalleri, and P. Ugliengo, Chem. Mater. **20**, 2522 (2008).
[33] J. C. Fogarty, P. Beck, H. M. Aktulga, A. Y. Grama, A. C. T. van Duin, and S. A. Pandit, J. Chem. Phys. **132**, 174704 (2010).
[34] P. Brommer, P. Beck, A. Chatzopoulos, F. Gähler, J. Roth, and H.-R. Trebin, J. Chem. Phys. **132**, 194109 (2010).
[35] S. J. Clark, M. D. Segall, C. J. Pickard, P. J. Hasnip, M. I. J. Probert, K. Refson, and M. C. Payne, Z. Kristallogr. **220**, 567 (2005).
[36] J. P. Perdew, Phys. Rev. B **33**, 8822 (1986).
[37] A. D. Becke, Phys. Rev. A **38**, 3098 (1988).
[38] D. R. Hamann, Phys. Rev. Lett. **76**, 660 (1996).
[39] P. Tangney and S. Scandolo, J. Chem. Phys. **119**, 9673 (2003).
[40] N. Bernstein, J. R. Kermode, and G. Csányi, Rep. Prog. Phys. **72**, 026501 (2009).
[41] G. Csányi, S. Winfield, J. Kermode, A. Comisso, A. De Vita, N. Bernstein, and M. C. Payne, "Expressive programming for computational physics in Fortran 95+," in *IoP Comput. Phys. Newsletter, Spring 2007* (2007). See http://www.libatoms.org.
[42] A. Togo, F. Oba, and I. Tanaka, Phys. Rev. B **78**, 134106 (2008).
[43] K. Kunc and R. Martin, Phys. Rev. Lett. **48**, 406 (1982).
[44] K. Parlinski, Z. Li, and Y. Kawazoe, Phys. Rev. Lett. **78**, 4063 (1997).
[45] K. Refson, P. Tulip, and S. Clark, Phys. Rev. B **73**, 155114 (2006).
[46] M. Born and K. Huang, *Dynamical Theory of Crystal Lattices* (Oxford University Press, Oxford, 1954).
[47] X. J. Han, L. Bergqvist, P. H. Dederichs, H. Müller-Krumbhaar, J. K. Christie, S. Scandolo, and P. Tangney, Phys. Rev. B **81**, 134108 (2010).
[48] M. Szymanski, A. Shluger, and A. Stoneham, Phys. Rev. B **63**, 224207 (2001).
[49] R. Van Ginhoven, H. Jónsson, and L. Corrales, Phys. Rev. B **71**, 024208 (2005).
[50] A. Roder, W. Kob, and K. Binder, J. Chem. Phys. **114**, 7602 (2001).